MNRAS 000, 1–13 (2025) Preprint 8 August 2025 Compiled using MNRAS LATEX style file v3.0



# Constraints on transition redshift utilizing the latest H(z) measurements and comments on the Hubble tension

J. P. Hu[1,2]⋆, X. D. Jia[2], D. H. Gao[2], J. Z. Gao[3], B. Q. Gao[4] and F. Y. Wang[2,5]†
[1] *Ministry of Education Key Laboratory for Nonequilibrium Synthesis and Modulation of Condensed Matter, School of Physics, Xi'an Jiaotong University, Xi'an 710049, China*
[2] *School of Astronomy and Space Science, Nanjing University, Nanjing 210093, China*
[3] *Institute of Theoretical Physics, School of Physics, Dalian University of Technology, Dalian 116024, China*
[4] *Research Center for Astronomical Computing, Zhejiang Lab, Hangzhou, 311100, China*
[5] *Key Laboratory of Modern Astronomy and Astrophysics (Nanjing University), Ministry of Education, Nanjing 210093, China*

Accepted XXX. Received YYY; in original form ZZZ

**ABSTRACT**

The motivation of this paper is to obtain reliable constraints of transition redshift ($z_{ztr}$) and, in combination with the evolution of the Hubble constant ($H_0$) that could alleviate the Hubble tension, discuss the possible origin of the tension. Utilizing the latest H(z) measurements and different methods (ΛCDM model, Cosmography, and Gaussian process method), we investigated the impact of methodology and dataset on $z_{ztr}$ constraints, and find that the choice of method has a greater impact on $z_{tr}$ than the observations themselves. Through a statistical analysis of the $z_{ztr}$ constraints from 2004 to 2024, we find that total $z_{tr}$ constraints (2004−2024) can be well described by a Gaussian function with the mean value 0.65 and the standard deviation 0.16; that is, $\bar{z}_{tr}(\text{all}) = 0.65 \pm 0.16$. And we confirmed that both dataset and methodology can indeed significantly affect the final constraints. The screened $z_{tr}$ constraints with free $H_0$ gives a new result $\bar{z}_{tr}(\text{free}) = 0.64 \pm 0.16$. Coincidentally, the $z_{tr}$ results overlap with the initial moment of $H_0$ evolution ($H_0$ value starts to deviate from the Planck result). This may suggest that the Hubble tension might be closely related to this particular period in the evolution of the Universe.

**Key words:** cosmological parameters – cosmology: theory – cosmology: observations – Cosmology

## 1 INTRODUCTION

Most observations indicate that the Universe is currently in a phase of accelerated expansion, including type Ia supernovae (SNe Ia; Riess et al. 1998, 2007; Scolnic et al. 2018; Brout et al. 2022; Rubin et al. 2023; Abbott et al. 2024), Cosmic Microwave Background (CMB; Komatsu et al. 2011; Planck Collaboration et al. 2014, 2020a), Baryonic Acoustic Oscillations (BAOs; Eisenstein et al. 2005; Roos 2012; Eisenstein et al. 2011; Smee et al. 2013; Adame et al. 2025b), Hubble parameter (H(z)) measurements (Farooq et al. 2013b; Farooq & Ratra 2013; Farooq et al. 2017; Sudharani et al. 2024; Koussour et al. 2024), Gamma-ray bursts (GRBs; Wang et al. 2015; Hu et al. 2021; Cao et al. 2022a; Wang et al. 2022; Liu et al. 2022; Jia et al. 2022; Dainotti et al. 2023), Dark energy survey (DES; Abbott et al. 2019), quasar lensing (Wong et al. 2020) and so on. The so-called ΛCDM model is the simplest theoretical model that supports this acceleration phase, which consists of a cosmological constant Λ term (Weinberg 1989; Padmanabhan 2003) and a cold dark matter component (Davis et al. 1985; Silk et al. 2010). In addition, there are several other models that can also explain the accelerated expansion, such as dark energy fluid (Peebles & Ratra 2003), massive gravity theories (Volkov 2012), modifications of Newtonian theory (MOND; Milgrom 1983), f(R) gravity (Capozziello & de Laurentis 2011; Guo & Frolov 2013), f(T) gravity (Myrzakulov 2011; Cai et al. 2016), brane world models (Cline et al. 1999; Randall & Sundrum 1999), string (Damour & Polyakov 1994), Kaluza-Klein theories (Overduin & Wesson 1997), and so on. Theoretically, the current accelerated expansion of the Universe is a smooth transition from a decelerating expansion. A model without a deceleration-acceleration transition fails on explaining current cosmological observations (Jesus et al. 2020).

Since the discovery of the accelerated expansion of

⋆ E-mail: hjp1206@163.com
† E-mail: fayinwang@nju.edu.cn

the Universe (Riess et al. 2004), there have been many attempts, using different type observations and methods, to precisely constrain the parameter that determines such transition from deceleration to an accelerated phase, that is transition redshift $z_{tr}$ (Firmani et al. 2005; Liang & Zhang 2005; Guimarães et al. 2009; Rani et al. 2015; Yu et al. 2018; Capozziello et al. 2022; Rahman 2023). Various approaches have been proposed and can be roughly divided into two categories: (i) model-dependent and (ii) model-independent. The former (i) gives the constraints of $z_{tr}$ based on commonly cosmological models, for example ΛCDM (Firmani et al. 2005), $w_0$CDM (Firmani et al. 2005), oΛCDM (Moresco et al. 2016), Chevallier-Polarski-Linder (CPL) model(Krishnan et al. 2021), Chameleon model (Salehi & Hatami 2022). The latter (ii) usually adopts a model-independent method to constrain the parameter $z_{tr}$, for instance Cosmograhpy (Riess et al. 2004, 2007; Guimarães et al. 2009), linear parametrization (Cunha & Lima 2008; Rani et al. 2015; Jesus et al. 2018; Muccino et al. 2023), Gaussian process (GP; Seikel et al. 2012; Yu et al. 2018; Kumar et al. 2023), piecewise linear fit (Moresco et al. 2016), and Bezier curve (Muccino et al. 2023). In theory, for the given cosmic evolution history, consistent constraints should be given on the transition redshift $z_{tr}$ when using different methods and different type of observations. For the determination of transition redshift $z_{tr}$, it is important for understanding the late-time evolution history of the Universe. Until now, the local observations can not provide accurate constraints on $z_{tr}$ like the CMB and the their distribution is relatively scattered, most of which fall within the redshift range (0.3, 1.0). In order to accurately estimate the transition redshift, much high-quality data at high enough redshift above the transition redshift are needed. At the same time, different methods and observations are also necessary to facilitate cross-verification.

Recently, there have been some hints that the Hubble constant $H_0(z)$ might evolve with the redshift of the data used. They come from a combination of different observations and methods, and the main observations used include quasar lens (Wong et al. 2020; Millon et al. 2020), SNe Ia (Dainotti et al. 2021; Horstmann et al. 2022; Malekjani et al. 2024; Ó Colgáin et al. 2024; Dainotti et al. 2025), H(z) measurements (Hu & Wang 2022a), and composite observations (Krishnan et al. 2020; Dainotti et al. 2022; Ó Colgáin et al. 2022; Jia et al. 2023; Xu et al. 2024; Jia et al. 2025; Lopez-Hernandez & De-Santiago 2025). The evolutionary behavior of $H_0(z)$ is one of the proposed solutions that can alleviate the Hubble tension which is currently one of the most serious challenge to the standard ΛCDM model. This tension arises from the 5$\sigma$ discrepancy between the values of $H_0$ measured from the local distance ladder (SH0ES; Riess et al. 2022) and the Planck cosmic microwave background (CMB; Planck Collaboration et al. 2020b). More information about the Hubble tension can be obtained from the review literature (Di Valentino et al. 2021; Abdalla et al. 2022; Perivolaropoulos & Skara 2022; Hu & Wang 2023; Kroupa et al. 2023; Vagnozzi 2023; Capozziello et al. 2024; Riess & Breuval 2024; Wang et al. 2024). It is noteworthy that the evolutionary behavior occurs at redshifts between 0.30 and 0.70 (Hu & Wang 2022a; Jia et al. 2023, 2025), which seems to coincide with the possible redshift range of the transition redshift $z_{tr}$. This may not be a coincidence. There are reasons to suspect that the Hubble tension might be related to this special period in the evolution of the Universe (Riess et al. 2004, 2007; Hu & Wang 2022a). Therefore, accurately constraining $z_{tr}$ might help us better understand the evolution of the Hubble constant and explore the nature of the Hubble tension.

In this present work, our primary goal is to constrain the transition redshift $z_{tr}$ utilizing the different combinations of methods and observations. Afterwards, we collected the results from studies from 2004 to 2024 and constructed a statistical analysis. Finally, based the final results and recent research on the evolution behavior of the Hubble constant that can alleviate the Hubble tension, we gave some comments on the tension. Our research encompasses three methods (ΛCDM model, Cosmography and Gaussian process (GP) method) and three kinds of H(z) measurements including cosmic chronometers (CCs), BAOs, and Dark Energy Spectroscopic Instrument (DESI) BAOs (Adame et al. 2025b). The outline of this paper is as follows. Section 2 provides basic information about the datasets used. Section 3 presents the methods for deriving estimates of $z_{tr}$ in detail. Section 4 contains the presentation of our principal results. A comprehensive analysis and discussion can be found in Sect. 5. Finally, a brief conclusion is presented in Sect. 6.

## 2 DATA SAMPLE

There are 60 H(z) measurements used in this paper. It covers redshift range (0.07, 2.40), consists 35 CCs (Moresco et al. 2012; Borghi et al. 2022; Jiao et al. 2023; Jimenez et al. 2023; Tomasetti et al. 2023a) and 25 BAOs (Hu et al. 2024c; Yang et al. 2024). The former is derived by comparing relative ages of galaxies at different redshifts (Jimenez & Loeb 2002). The latter depends on the sound horizon at the drag epoch $r_d$ (Adame et al. 2025b). More detailed information can be found in Tables A1 and A2. These two datasets have been widely used in cosmological researches, such as cosmological constraints (Yu et al. 2018; Briffa et al. 2020; Velasquez-Toribio & Magnago 2020; Cao et al. 2022b; Luongo & Muccino 2024), cosmic anisotropy (Bengaly et al. 2024; Hu et al. 2024b; Sah et al. 2024), calibration of the GRB correlations (Wang et al. 2015; Hu et al. 2021; Liang et al. 2022; Wang et al. 2022; Li et al. 2023; Favale et al. 2024), constraints of the transition redshift (Moresco et al. 2016; Jesus et al. 2020), cosmographic constraints (Li et al. 2020; Arjona & Nesseris 2021; Velasquez-Toribio & Fabris 2022) and alleviation of the Hubble tension (Hu & Wang 2022a; De Simone et al. 2024; Hu et al. 2024c; Liu et al. 2024a,b; Xu et al. 2024; Boubel et al. 2025; Lopez-Hernandez & De-Santiago 2025).

Uncertainty in the H(z) measurements consists of two components: statistical and systematic errors. The former will decrease with the advancement of observation technology and the increase of sample size, but the latter will not necessarily decrease accordingly. Systematic error can arise from a variety of factors, including instrumentation, environment, and observational methods. For CCs measurements, the systematic errors primarily stem from the assumption of stellar population synthesis (SPS) model, error in the CC star formation history (SFH), error in the CC metallicity estimate and rejuvenation effect (Moresco et al. 2022). For

BAOs measurements, the systematic errors primarily stem from theoretical systematics, modelling choices and observational systematics (Chen et al. 2024). For the treatments of systematic of CCs and BAOs, see references Moresco et al. (2020) and Gómez-Valent et al. (2024), respectively. In this paper, we not only considered statistical errors in the research process, but also analyzed and discussed the possible impact of systematic errors with examples.

## 3 METHODOLOGY

In this section, we will show how to reconstruct the deceleration parameter, q(z), from H(z) measurements, and then find the transition redshift from the condition $q(z_{tr}) = 0$. In order to perform this reconstruction, we must know how to obtain q(z) from H(z) measurements utilizing different approaches including the ΛCDM model, Cosmography, and GP method. Assuming a Friedman-Lemaitre-Robertson-Walker (FLRW) metric, the definition of the deceleration parameter q(z) and its relation to H(z) can be given by:

$$q(z) \equiv -\frac{1}{H^2}\frac{\ddot{a}}{a} = \frac{1+z}{H}\frac{dH}{dz} - 1, \tag{1}$$

where $a$ is the scale factor, and H is Hubble parameter H(z). As one may see, the deceleration parameter q(z) can be obtained from H(z) and from its first derivative, $H^{'}(z)$.

### 3.1 ΛCDM model

For the flat ΛCDM model, H(z) can be given by

$$H(z) = H_0 E(z) = H_0\sqrt{\Omega_m(1+z)^3 + \Omega_\Lambda}. \tag{2}$$

Here $H_0$ is the Hubble constant, which characterizes the current expansion rate of the Universe. Parameters $\Omega_m$ and $\Omega_\Lambda$ represent the matter density and the dark energy density, respectively. In the flat ΛCDM model, the sum of these two parts equals 1.00, that is $\Omega_m + \Omega_\Lambda = 1$. Substituting Eqs. (2) into (1), we get

$$q(z) = -\frac{3\Omega_m(1+z)^3}{2[\Omega_m(1+z)^3 + 1 - \Omega_m]} - 1. \tag{3}$$

Utilizing Eq. (3), we can get the expression of transition redshift as follows

$$z_{tr} = [\frac{2(1-\Omega_m)}{\Omega_m}]^{1/3} - 1, \tag{4}$$

and its corresponding 1σ error is given by

$$\sigma_{z_{tr}} = \frac{2}{3}[\frac{2(1-\Omega_m)}{\Omega_m^4}]^{-\frac{2}{3}} \times \sigma_{\Omega_m}, \tag{5}$$

where $\sigma_{\Omega_m}$ represents the 1σ error of the best fits of $\Omega_m$. Finally, the estimation of the transition redshift $z_{tr}$ can be given by combining Eqs. (4) and (5) with the best fitting results of $\Omega_m$. Parameter fitting is performed employing the MCMC method, which introduced in detail in section 3.4.

### 3.2 Cosmography

Cosmography has been widely used in cosmological data processing to stint the state of the kinematics of our Universe in a model-independent way (Visser 2015; Dunsby & Luongo 2016; Capozziello et al. 2018; Capozziello & Ruchika 2019; Capozziello et al. 2019; Lusso et al. 2019; Bargiacchi et al. 2021; Gao et al. 2024; Kalbouneh et al. 2024, 2025; Mishra et al. 2025; Pourojaghi et al. 2025). It relies only on the assumption of a homogeneous and isotropy universe as described by the FLRW metric (Weinberg 1972). Its methodology is essentially based on expanding measurable cosmological quantities as Taylor series with respect to the current time. In this framework, the evolution of universe can be described by some cosmographic parameters, such as Hubble parameter $H$, deceleration $q$, jerk $j$, snap $s$, and lerk $l$ parameters. The corresponding definitions of these parameters can be expressed as follows:

$$H = \frac{\dot{a}}{a}, q = -\frac{1}{H^2}\frac{\ddot{a}}{a}, j = \frac{1}{H^3}\frac{\dddot{a}}{a}, s = \frac{1}{H^4}\frac{\ddddot{a}}{a}, l = \frac{1}{H^5}\frac{\overset{\cdots\cdot\cdot}{a}}{a}. \tag{6}$$

The $z$-redshift method is the earliest Taylor series used in Cosmography. The corresponding luminosity distance can be conveniently expressed as (Cattoën & Visser 2007; Capozziello et al. 2011)

$$\begin{aligned} d_L(z) &= \frac{c}{H_0}[z + \frac{1}{2}(1-q_0)z^2 - \frac{1}{6}(1 - q_0 - 3q_0^2 + j_0)z^3 \\ &+ \frac{1}{24}(2 - 2q_0 - 15q_0^2 - 15q_0^3 + 5j_0 + 10q_0j_0 + s_0)z^4 \\ &+ \frac{1}{120}(-6 + 6q_0 + 81q_0^2 + 165q_0^3 + 105q_0^4 + 10j_0^2 \\ &- 27j_0 - 110q_0j_0 - 105q_0^2j_0 - 15q_0s_0 - 11s_0 - l_0)z^5 \\ &+ O(z^6)], \end{aligned} \tag{7}$$

where $H_0$, $q_0$, $j_0$, $s_0$, and $l_0$ represent the current values. The first two terms above are Weinberg's version of the Hubble law which can be found from Equation (14.6.8) in the book (Weinberg 1972). The third and fourth terms are equivalent to that obtained by Nakamura & Chiba (1999) and Visser (2004), respectively. Meanwhile, the corresponding expression of H(z) can be written as (Capozziello et al. 2020b)

$$\begin{aligned} H(z) &= H_0[1 + (1+q_0)z + \frac{1}{2}(j_0 - q_0^2)z^2 - \frac{1}{6}(-3q_0^2 - 3q_0^3 \\ &+ j_0(3+4q_0) + s_0)z^3 + \frac{1}{24}(-4j_0 + l_0 - 12q_0^2 - 24q_0^3 \\ &- 15q_0^4 + j0(12 + 32q_0 + 25q_0^2) + 8s_0 + 7q_0s_0)z^4 \\ &+ O(z^5)]. \end{aligned} \tag{8}$$

Substituting Eqs. (8) in (1), we get

$$q(z) = \frac{p_1 + 2p_2z + (3p_3 + p_2)z^2 + (4p_4 + 2p_3)z^3 + 3p_4z^4}{1 + p_1z + p_2z^2 + p_3z^3 + p_4z^4}, \tag{9}$$

where

$$\begin{aligned} p_1 &= 1 + q_0, \\ p_2 &= \frac{1}{2}(j_0 - q_0^2), \\ p_3 &= -\frac{1}{6}(-3q_0^2 - 3q_0^3 + j_0(3+4q_0) + s_0), \\ p_4 &= \frac{1}{24}(-4j_0 + l_0 - 12q_0^2 - 24q_0^3 - 15q_0^4 + j0(12 + 32q_0 \\ &+ 25q_0^2) + 8s_0 + 7q_0s_0)z^4. \end{aligned} \tag{10}$$

Considering the small amount of data, in order to avoid overfitting and high uncertainty, we only give constraints on first two parameters $q_0$ and $j_0$ (Hu & Wang 2022b). With the simplified Eqs. (8) and (9), we can derive the transition redshift according to the condition q($z_{tr}$) = 0 in the following form

$$z_{tr} = -1 + \sqrt{1 + \frac{-2q_0}{j_0 - q_0^2}}. \tag{11}$$

The corresponding $1\sigma$ error can be given by

$$\sigma_{z_{tr}} = \frac{1}{2}(1 + \frac{-2q_0}{j_0 - 2q_0^2})^{-1/2} \times [(\frac{-2j_0 - 2q_0^2}{(j_0 - q_0^2)^2})^2 \sigma_{q_0}^2 + (\frac{-2q_0}{(j_0 - q_0^2)^2})^2 \sigma_{j_0}^2]^{1/2}, \tag{12}$$

where $\sigma_{q_0}$ and $\sigma_{j_0}$ are the $1\sigma$ errors corresponding to the best fits.

### 3.3 Gaussian process method

Gaussian process has been extensively used for cosmological applications, such as constraint on cosmological parameters (Yu et al. 2018; Gómez-Valent & Amendola 2018; Liao et al. 2019; Briffa et al. 2020), calibration of high redshift cosmic probe (Hu et al. 2021; Wang et al. 2022) and comparison of cosmological models (Melia & Yennapureddy 2018). Here, we only give a brief introduction to the GP method. A more detailed explanation can be discovered from the literature (Rasmussen & Williams 2006; Schulz et al. 2018). In this work, the GP regression is implemented by employing the package *GaPP3* [1] (Pedregosa et al. 2011) in the Python environment. It will reconstruct a continuous function $h(x)$ that is the best representative of a discrete set of measurements $h(x_i) \pm \sigma_i$ at $x_i$, where $i$ = 1,2,..., $N$ and $\sigma_i$ is the $1\sigma$ error. The GP method assumes that the value of $h(x_i)$ at any position $x_i$ is random that follows a Gaussian distribution with expectation $\mu(x)$ and standard deviation $\sigma(x)$. They can be determined from observations through a defined covariance function $k(x, x_i)$ or kernel function

$$\mu(x) = \sum_{i,j=1}^{N} k(x, x_i)(M^{-1})_{ij} h(x_j), \tag{13}$$

and

$$\sigma(x) = k(x, x_i) - \sum_{i,j=1}^{N} k(x, x_i)(M^{-1})_{ij} k(x_j, x), \tag{14}$$

where the matrix $M_{ij} = k(x_i, x_j) + c_{ij}$ and $c_{ij}$ is the covariance matrix of the observations. For uncorrelated data, it can be simplified as $diag(\sigma_i^2)$. Equations (13) and (14) specify the posterior distribution of the extrapolated points. For given data sets $(x_i, y_i)$, considering a suitable GP kernel, it is straightforward to derive the continuous function $h(x)$ which used to get the value of $H_0$, that is $h(0)$.

In this work, we consider a common kernel function, the Radial Basis Function kernel (RBF) kernel, also known as the Gaussian kernel, which can be written as

$$k(x, \tilde{x}) = \sigma_h^2 \exp\left[-\frac{(x - \tilde{x})^2}{2l^2}\right], \tag{15}$$

where, parameters $\sigma_h$ and $l$ control the strength of the correlation of the function value and the coherence length of the correlation in $x$, respectively. More detailed information about covariance functions for the Gaussian process can be found in chapter 4 of the book (Rasmussen & Williams 2006). Parameters $\sigma_h$ and $l$ are optimized for the observations, $h(x_i) \pm \sigma_i$, by minimizing the log marginal likelihood function (Seikel et al. 2012)

$$\ln \mathcal{L} = -\frac{1}{2} \sum_{i,j=1}^{N} [h(x_i) - \mu(x_i)](M^{-1})_{ij}[h(x_j) - \mu(x_j)] - \frac{1}{2} \ln |M| - \frac{1}{2} N \ln 2\pi, \tag{16}$$

where $|M|$ is the determinant of $M_{ij}$.

The GP method, as performed by GaPP3, furnish not only the H(z) reconstruction from H(z) measurements, but also its derivatives up to fourth order and their estimated uncertainties and covariances. More details can be found from Seikel et al. (2012). Therefore, it just remains to estimate the uncertainty of q(z), $\sigma_q$, via the error propagating Eq. (1). We get

$$q(z) = \frac{1+z}{H} H' - 1, \tag{17}$$

and

$$(\frac{\sigma_q}{1+q})^2 = (\frac{\sigma_{H'}}{H'})^2 + (\frac{\sigma_H}{H})^2 - \frac{2\sigma_{HH'}}{HH'}, \tag{18}$$

where, $H'$ represents the derivative of H(z) with respect to redshift z.

### 3.4 MCMC method

Constraints of free parameters $P_i$ (including $\Omega_m$, $H_0$, $q_0$ and $j_0$) for a fixed cosmological model can be given by minimizing the chi-square ($\chi^2$) function. When only statistical error is considered, the corresponding format of $\chi^2$ is as follows:

$$\chi^2 = \sum_{i=1}^{N} \frac{(\Delta H)^2}{\sigma_i^2}. \tag{19}$$

Here, $\sigma_i$ is the corresponding $1\sigma$ statistical error. $\Delta H$ represents the difference between the observational Hubble parameter $H_{\rm obs}(z)$ and the theoretical prediction $H_{\rm th}(P_i, z_i)$:

$$\Delta H = H_{\rm obs}(z) - H_{\rm th}(P_i, z_i). \tag{20}$$

Equations (2) and (8) can provide the $H_{\rm th}(P_i, z_i)$ for the flat ΛCDM model and the Cosmography method, respectively. When both statistical error ($C_{\rm stat}$) and systematic error ($C_{\rm syst}$) are considered, the corresponding format of $\chi^2$ is as follows:

$$\chi^2 = \Delta H C_{\rm stat+syst}^{-1} \Delta H^T. \tag{21}$$

At this time, the statistical ($C_{stat}$) and systematic ($C_{syst}$) covariance matrices are combined and adopted to constrain the cosmological parameters:

$$C_{\rm stat+syst} = C_{\rm syst} + C_{\rm stat}. \tag{22}$$

In this work, the minimization is performed employing a Bayesian Markov chain Monte Carlo (MCMC) (Foreman-Mackey et al. 2013) method with the *emcee* package[2]. All

[1] https://github.com/lighink/GaPP3

[2] https://emcee.readthedocs.io/en/stable/

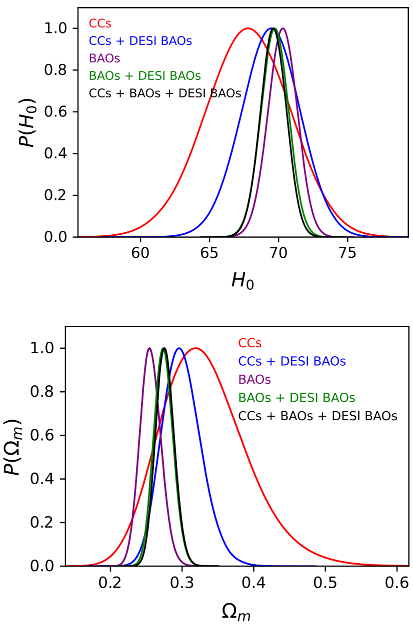


**Figure 1.** Cosmological constraints of the flat ΛCDM model from a diverse combination of observations which consists CCs, BAOs and DESI BAOs.

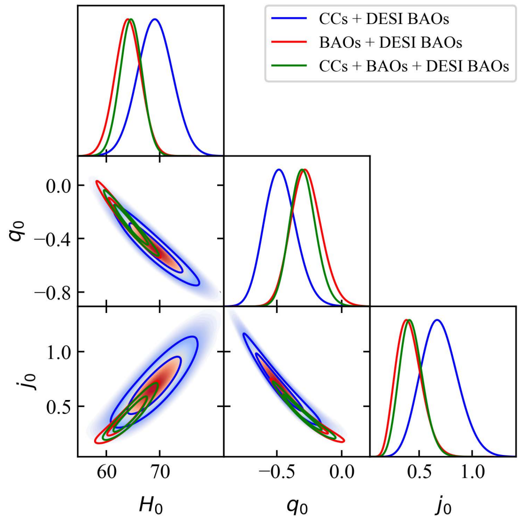


**Figure 2.** Confidence contours ($1\sigma$ and $2\sigma$) for the parameters space ($H_0$, $q_0$, $j_0$) utilizing the Cosmography method.

the fittings in this paper are obtained adopting this python package.

## 4 RESULTS

First, we gave the cosmological constraints of the ΛCDM model from a diverse combination of observations which including CCs, BAOs and DESI BAOs. For the CCs + BAOs + DESI BAOs combination, the corresponding constraints are $\Omega_m = 0.28 \pm 0.01$ and $H_0 = 69.63 \pm 0.94$ km/s/Mpc. They are in line with ones obtained from other combinations within $1\sigma$ level. All the marginalized likelihood distributions are shown in Fig. 1 and the corresponding best fits are summarized in Table 1. According to the cosmological constraints, we derived the corresponding $z_{tr}$ estimations utilizing the Eqs. (4) and (5). Results derived from various combinations are 0.60±0.13 (CCs), 0.67±0.08 (CCs + DESI BAOs), 0.79±0.05 (BAOs), 0.76±0.03 (BAOs + DESI BAOs) and 0.73±0.03 (CCs + BAOs + DESI BAOs).

For the estimation of $z_{tr}$ based on the Cosmography, we still need to first give the cosmographic constraints on different observational combinations. Subsequently, by inserting the best fits into Eqs. (11) and (12), the estimations of $z_{tr}$ can be achieved. Individual CCs or BAOs measurements do not give tight constraints here. Thus, we only considered three combination scenarios: (1) CCs + DESI BAOs, (2) BAOs + DESI BAOs and (3) CCs + BAOs + DESI BAOs. The best fitting results are ($H_0$ = $69.11^{+3.31}_{-3.28}$ km/s/Mpc, $q_0$ = -$0.48^{+0.13}_{-0.12}$, $j_0$ =$0.69^{+0.18}_{-0.17}$), ($H_0$ = $64.03^{+2.44}_{-2.43}$ km/s/Mpc, $q_0$ = -$0.28^{+0.12}_{-0.11}$, $j_0$ = $0.40^{+0.13}_{-0.11}$) and ($H_0$ = 64.61±2.08 km/s/Mpc, $q_0$ = -0.30±0.10, $j_0$ = $0.42^{+0.12}_{-0.10}$) for the observational combinations CCs + DESI BAOs, BAOs + DESI BAOs and CCs + BAOs + DESI BAOs, respectively. The corresponding confidence contours and best fits are shown in Fig. 2 and Table 1, respectively. According the Cosmographic constraints, we gave the final estimations of $z_{tr}$: (1) 0.45±0.38, (2) 0.32±0.38 and (3) 0.35±0.33.

For the GP method, we first drew the reconstructed H(z) function with $1\sigma$ error based on the different observational combinations, as shown in Fig. 3. Utilizing the reconstruction function of H(z), it is convenient to obtain the estimates of $H_0$. The $H_0$ constraints are overall biased towards Planck results (Planck Collaboration et al. 2020a). The numerical results are summarized in Table 1. Combining the reconstructed functions of H(z) and $H^{'}$(z) with Eqs. (17) and (18), we can reconstruct the q(z) function. From the reconstructed results in Fig. 4, it is easy to get the transition redshift employing the condition $q(z_{tr}) = 0$, and the estimation of $q_0$. The estimations of $q_0$ from CCs, CCs + DESI BAOs, BAOs, BAOs + DESI BAOs, CCs + BAOs + DESI BAOs datasets are -0.49±0.44, -0.55±0.26, -0.25±0.12, -0.34±0.13, and -0.39±0.14, respectively. These $q_0$ values are consistent with the result of standard ΛCDM model with $\Omega_m = 0.30$. The results of the transition redshift $z_{tr}$ are $0.57^{+0.13}_{-0.23}$ (CCs), $0.72^{+0.07}_{-0.08}$ (CCs + DESI BAOs), $0.58^{+0.15}_{-0.26}$ (BAOs), $0.63^{+0.09}_{-0.13}$ (BAOs + DESI BAOs) and $0.65^{+0.07}_{-0.09}$ (CCs + BAOs + DESI BAOs).

In addition, we also gave the results considering the systematic error to discuss the influence of the systematic error on the $z_{tr}$ constraints. Taking CCs + DESI BAOs sample as an example, we gave the constraints obtained by different methods when considering the CCs systematic and statistical errors, as shown in Table 2. For the ΛCDM model, Cosmography and GP method, the estimations of $z_{tr}$ are 0.69±0.08, 0.50±0.44 and $0.77^{+0.07}_{-0.09}$, respectively. In here, the system covariance matrix of CCs is calculated utilizing the method proposed by Moresco et al. (2020), which combines statistical and systematic errors. These covariance matrices have been widely used in cosmological researches (Gómez-Valent et al. 2024; Ó. Colgáin et al. 2025).

**Table 1.** Cosmological constraints ($\Omega_m$, $H_0$, $q_0$ and $j_0$) and derived estimations ($z_{tr}$) utilizing different combinations of methods and datasets. Parameter $H_0$ in units of km s$^{-1}$Mpc$^{-1}$.

| Method | Parameter | Dataset (A) | Dataset (B) | Dataset (C) | Dataset (D) | Dataset (E) |
|---|---|---|---|---|---|---|
| flat ΛCDM | $H_0$ | $67.76^{+3.04}_{-3.09}$ | $69.44^{+2.10}_{-2.13}$ | $70.29^{+1.05}_{-1.06}$ | $69.72^{+0.99}_{-1.00}$ | 69.63±0.94 |
| | $\Omega_m$ | $0.33^{+0.06}_{-0.05}$ | 0.30±0.03 | $0.26^{+0.02}_{-0.01}$ | 0.27±0.01 | 0.28±0.01 |
| | $z_{tr}$ | 0.60±0.13 | 0.67±0.08 | 0.79±0.05 | 0.76±0.03 | 0.73±0.03 |
| Cosmography | $H_0$ | – | $69.11^{+3.31}_{-3.28}$ | – | $64.03^{+2.44}_{-2.43}$ | 64.61±2.08 |
| | $q_0$ | – | $-0.48^{+0.13}_{-0.12}$ | – | $-0.28^{+0.12}_{-0.11}$ | -0.30±0.01 |
| | $j_0$ | – | $0.69^{+0.18}_{-0.17}$ | – | $0.40^{+0.13}_{-0.11}$ | $0.42^{+0.12}_{-0.10}$ |
| | $z_{tr}$ | – | 0.45±0.38 | – | 0.32±0.38 | 0.35±0.33 |
| GP | $H_0$ | 67.48 ± 4.58 | 70.19±3.58 | 63.17±3.11 | 64.97±2.68 | 67.79±4.48 |
| | $q_0$ | -0.49±0.44 | -0.55±0.26 | -0.25±0.12 | -0.34±0.13 | -0.39±0.14 |
| | $z_{tr}$ | $0.57^{+0.13}_{-0.23}$ | $0.72^{+0.07}_{-0.08}$ | $0.58^{+0.15}_{-0.26}$ | $0.63^{+0.09}_{-0.13}$ | $0.65^{+0.07}_{-0.09}$ |

Note: Dataset combination: (A) CCs; (B) CCs + DESI BAOs; (C) BAOs; (D) BAOs + DESI BAOs; (E) CCs + BAOs + DESI BAOs.

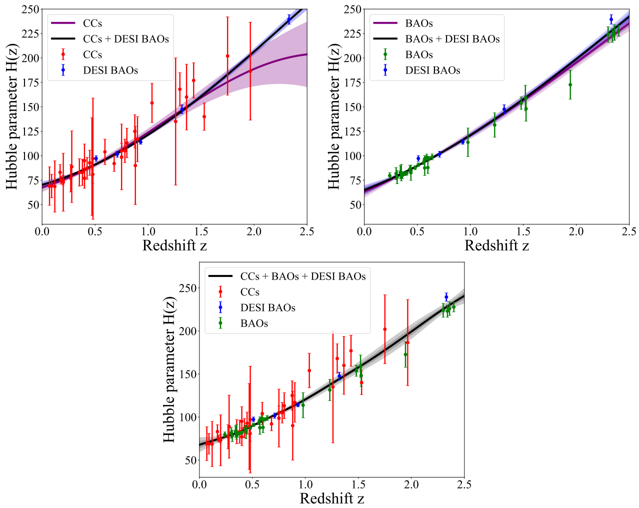


**Figure 3.** Reconstruction of the Hubble parameter H(z) adopting the GP method with different combinations of CCs, BAOs, DESI BAOs datasets.

**Table 2.** Cosmological constraints ($\Omega_m$, $H_0$, $q_0$ and $j_0$) and derived estimations ($z_{tr}$) obtained from CCs + DESI BAOs utilizing different methods, taking into account both CCs systematic and statistical errors. Parameter $H_0$ in units of km s$^{-1}$Mpc$^{-1}$.

| Method | Parameter | Dataset (B) |
|---|---|---|
| flat ΛCDM | $H_0$ | $70.31^{+2.48}_{-2.53}$ |
| | $\Omega_m$ | 0.29±0.03 |
| | $z_{tr}$ | 0.69±0.08 |
| Cosmography | $H_0$ | $70.98^{+4.06}_{-4.08}$ |
| | $q_0$ | $-0.53^{+0.14}_{-0.13}$ |
| | $j_0$ | $0.75^{+0.20}_{-0.19}$ |
| | $z_{tr}$ | 0.50±0.44 |
| GP | $H_0$ | 72.54±4.56 |
| | $q_0$ | -0.61±0.35 |
| | $z_{tr}$ | $0.77^{+0.07}_{-0.09}$ |

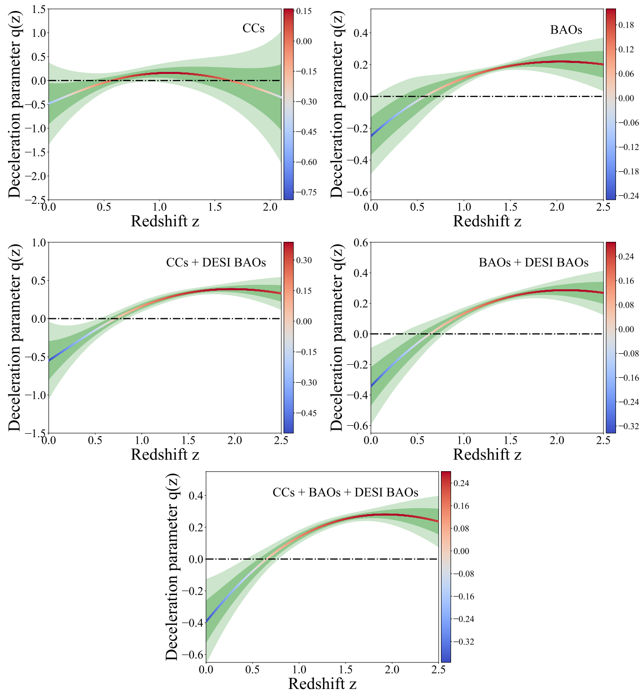


**Figure 4.** Reconstruction of the deceleration parameter q(z) adopting the GP method with different combinations of CCs, BAOs, DESI BAOs datasets.

## 5 ANALYSIS AND DISCUSSION

Full numerical results from our analysis are displayed in Table 1 and Fig. 5. The left panel of Fig. 5 is classified according to methodology, which helps to understand the discrepancy between different methods. The right panel shows the classification according to used samples. From Fig. 5, we can find that the $z_{tr}$ constraints obtained from different datasets employing the same approach are consistent with each other within $1\sigma$ level. Afterwards, we calculated the mean values $\tilde{z}_{tr}$ of the same method. For the flat ΛCDM, the result is $\tilde{z}_{tr} = 0.71 \pm 0.06$ ($\tilde{\sigma}_{z_{tr}}$). The ones from the Cosmography and GP method are $0.37 \pm 0.36$ and $0.63^{+0.10}_{-0.16}$, respectively. It can be found that $\tilde{z}_{tr}$(Cosmography) < $\tilde{z}_{tr}$(GP method) < $\tilde{z}_{tr}$(ΛCDM model) and $\tilde{\sigma}_{z_{tr}}$(ΛCDM model) <

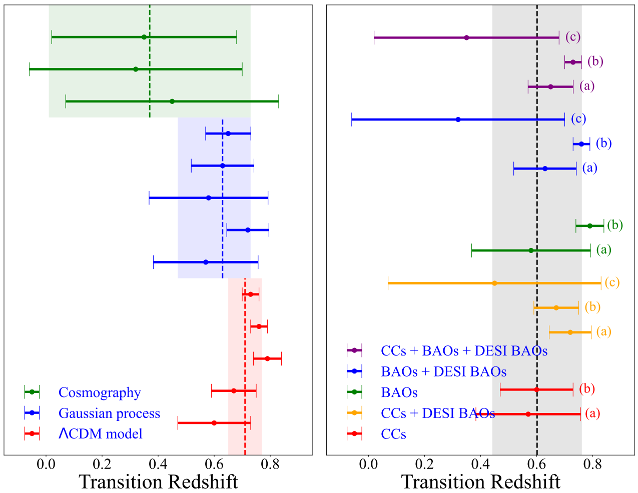


**Figure 5.** Estimations of the transition redshift $z_{tr}$ adopting the different methods with diverse combinations of of CCs, BAOs, DESI BAOs datasets. Left panel shows all the results classified by the approaches used. Dotted lines and shadow regions represent the mean value and corresponding $1\sigma$ range calculated by the results from different methods. For the flat $\Lambda$CDM model, Cosmography and GP method, the calculations are $\tilde{z}_{tr} = 0.71 \pm 0.06$, $0.37 \pm 0.36$ and $0.63^{+0.10}_{-0.16}$, respectively. Right panel shows all the results classified according to the dataset used. Labels (a), (b) and (c) represent the GP method, the flat $\Lambda$CDM model, and the Cosmography method, respectively. Dotted line and shadow regions represent the mean value and corresponding $1\sigma$ range calculated by all our results, that is $\tilde{z}_{tr} = 0.60 \pm 0.16$.

$\tilde{\sigma}_{z_{tr}}$(GP method) $<$ $\tilde{\sigma}_{z_{tr}}$(Cosmography). The results obtained by the model-independent method are significantly smaller than those of the $\Lambda$CDM model. Different methods have different abilities to constrain the transition redshift $z_{tr}$. The flat $\Lambda$CDM model and GP method give smaller $1\sigma$ error of $z_{tr}$ constraints than that from the Cosmography method. Cosmography method has more free parameters, which will make the constraints worse and increase the $1\sigma$ error of $z_{tr}$. From the right panel of Fig. 5, we can see that the impact of the dataset on the results is weaker than that of the methodology. Afterwards, we calculated the statistical mean of our results and its $1\sigma$ error; that is $\tilde{z}_{tr} = 0.60$ and $\tilde{\sigma}_{z_{tr}} = 0.16$. At the same time, we also investigated the impact of systematic errors on the results using CCs + DESI BAOs as an example. By comparing the results before and after considering the systematic error, as shown in Tables 1 and 2, we find that considering the systematic error can cause the best fits of the cosmological parameters ($\Omega_m$, $H_0$, $q_0$ and $j_0$) to change insignificantly (less than $1\sigma$), and the corresponding $1\sigma$ error increases slightly. Changes in constraints on cosmological parameters ($\Omega_m$, $q_0$ and $j_0$) lead to a slight increase (less than $1\sigma$) in the estimated value of $z_{tr}$. It is worth noting that the Hubble constant $H_0$ is the most affected, with a maximum increase of 2.35 km/s/Mpc, but it is not directly related to the estimation of $z_{tr}$. This finding shows that systematic errors can significantly affect the value of $H_0$, suggesting that the current Hubble tension might also be caused by unknown systematic errors. We should be cautious about systematic errors.

Since the discovery of the accelerated expansion of the Universe, there have been many researches on the transition redshift $z_{tr}$. Many $z_{tr}$ related researches (2004-2024) which utilizing different types of observations and approaches are showed in Table A3. According to the type of dataset and the methodology, we categorized the collected results, as shown in Fig. 6. The left panel shows the classification results according to the dataset, and the right panel shows the classification results according to the methodology. From Fig. 6, it is easy to find that our results are in line with with most of the results, with only a few being inconsistent (Rani et al. 2015; Jesus et al. 2018; Capozziello et al. 2022). Overall, current constraints on $z_{tr}$ are quite diffuse, covering a wide redshift range (0.25, 1.02). It can be seen that both the dataset and methodology can both affect the final result, with the latter having a stronger impact. Therefore, the current results of the constraints of $z_{tr}$ are still inconclusive. Through statistical analysis, we find that all $z_{tr}$ constraints (2004−2024) can be well described by a Gaussian function with the mean value 0.65 ($\bar{z}_{tr}$(all)) and the standard deviation 0.16 ($\sigma_{\bar{z}_{tr}}$(all)), as shown in Fig. 7.

From the left panel of Fig. 6, taking $\bar{z}_{tr}(\text{all}) = 0.65$ as reference, we can find that $z_{tr}$ constraints obtained from different type datasets have different preferences. Some datasets prefer smaller value, such as SNe Ia (Riess et al. 2004, 2007; Cunha & Lima 2008; Guimarães et al. 2009; Capozziello et al. 2015), CCs (Yu et al. 2018), CCs + two ly$\alpha$ (Yu et al. 2018). Some prefer larger value, for instant, GRBs (Liang & Zhang 2005; Wang & Dai 2006; Muccino et al. 2023), H(z) + SNe Ia (Jesus et al. 2018; Velasquez-Toribio & Magnago 2020), CCs + SNe Ia + ISW (Rahman 2023), BAOs (Busca et al. 2013). The rest show no clear preference (Firmani et al. 2005; Wang & Dai 2006; Cunha & Lima 2008; Xu et al. 2009; Planck Collaboration et al. 2020a). Compared with the dataset type, the preferences for different methods are more obvious. From right panel of Fig. 6, we can see the tendencies of different methods. The $z_{tr}$ constraints utilizing the flat $\Lambda$CDM model (Firmani et al. 2005; Liang & Zhang 2005; Wang & Dai 2006; Guimarães et al. 2009; Farooq et al. 2017; Planck Collaboration et al. 2020a; Velasquez-Toribio & Magnago 2020; Rahman 2023), f(R) gravity (Capozziello et al. 2014), linear parametrization (Cunha & Lima 2008; Rani et al. 2015; Jesus et al. 2018; Capozziello et al. 2022; Muccino et al. 2023), and statistical analysis (Farooq & Ratra 2013; Farooq et al. 2013a, 2017) favor a larger value. Ones from the $w_0$CDM model (Firmani et al. 2005), $w_z$CDM model (Firmani et al. 2005), Chameleon model (Salehi & Hatami 2022), f(T) gravity (Capozziello et al. 2015), GP method (Yu et al. 2018; Haridasu et al. 2018; Jesus et al. 2020), and Piecewise linear fit (Moresco et al. 2016) prefer a smaller value. In general, there are certain preferences for the $z_{tr}$ constraints given by different methods and different datasets. In addition to methods and observations, different treatments of nuisance parameter ($H_0$) can also affect the constraints of $z_{tr}$. In past studies, there are three common treatments: (a) fixed (Firmani et al. 2005; Liang & Zhang 2005; Wang & Dai 2006; Farooq & Ratra 2013; Farooq et al. 2013a, 2017), (b) marginalized (Cunha & Lima 2008; Moresco et al. 2016; Kumar et al. 2023), and (c) free (Riess et al. 2004; Xu et al. 2009; Jesus et al. 2018; Yu et al. 2018; Haridasu et al. 2018; Jesus et al. 2020; Muccino et al. 2023; Myrzakulov et al. 2024). Specifically, category (a) usually fixes $H_0$ to the mea-

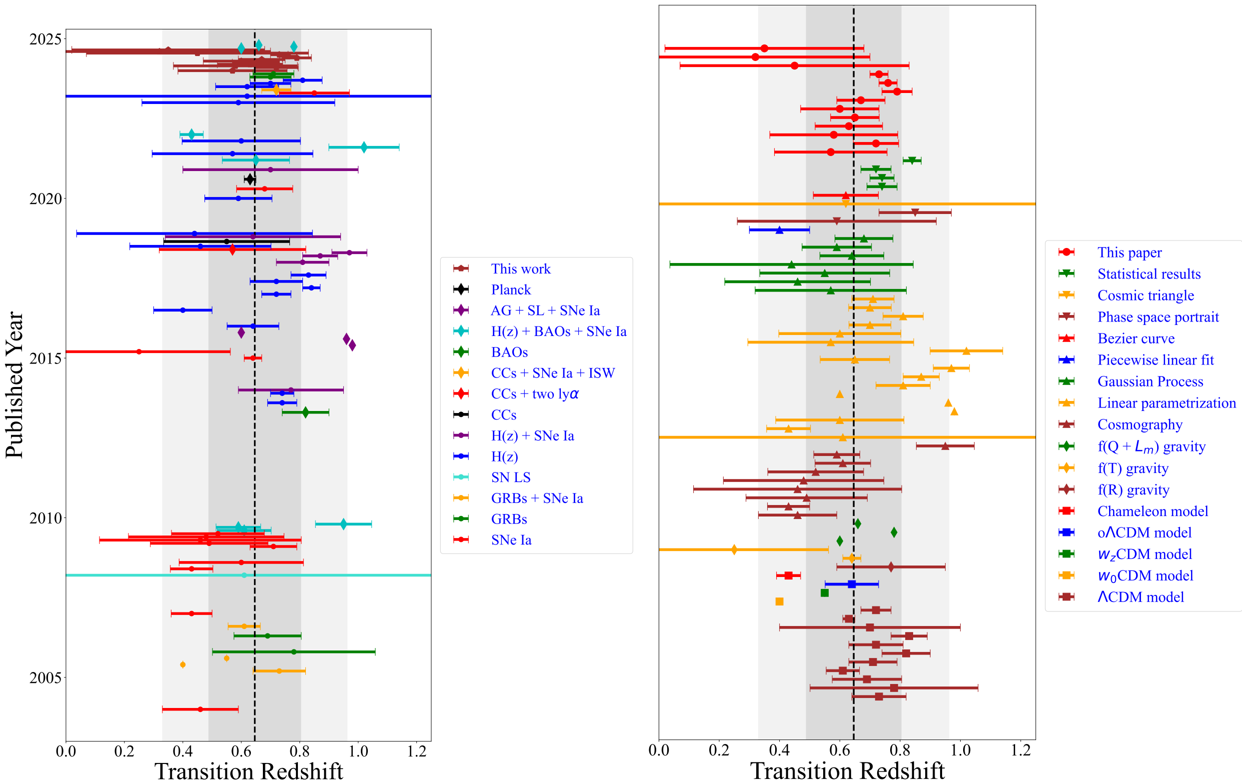


**Figure 6.** Estimations of transition redshift $z_{tr}$ obtained from different combinations of observations and methods. In the left panel, all $z_{tr}$ results are sorted by submitted year and the datasets used are marked. The right panel shows the result classified according to the analysis method. Black dotted line represents the mean value $\bar{z}_{tr} = 0.65$. The shaded regions represent the $1\sigma$ and $2\sigma$ ranges.

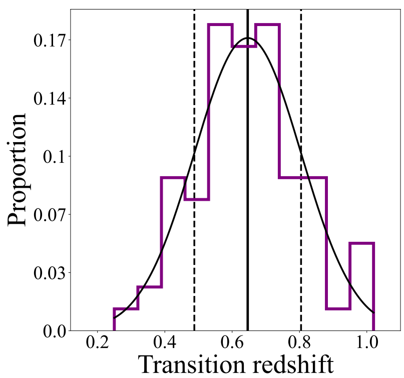


**Figure 7.** Statistical result of transition redshift $z_{tr}$ which obtained between 2004 and 2024. The $z_{tr}$ distribution well described by a Gaussian function with the mean value 0.65 (solid line) and the standard deviation 0.16 (dotted line).

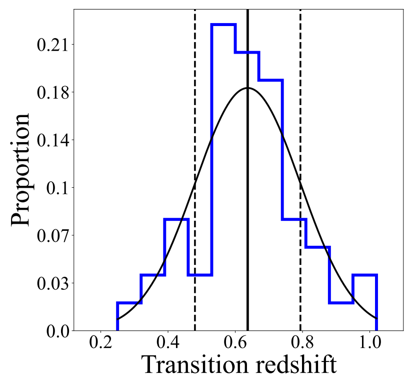


**Figure 8.** Statistical result of transition redshift $z_{tr}$ which obtained between 2004 and 2024 with free $H_0$. The $z_{tr}$ distribution well described by a Gaussian function with the mean value 0.64 (solid line) and the standard deviation 0.16 (dotted line).

surements of SH0ES (Riess et al. 2022) or CMB (Planck Collaboration et al. 2020a); category (b) typically assumes a Gaussian prior on $H_0$ based on the SH0ES (Riess et al. 2022) or CMB (Planck Collaboration et al. 2020a) results; and category (c) treats $H_0$ as a free parameter. Categories (a) and (c) are relatively easy to understand. For category (b), we give an example to help readers understand, for instance, Moresco et al. (2016) assumed a gaussian prior on the Hubble constant $H_0 = 73\pm2.4$ km/s/Mpc (Riess et al. 2011) to obtain the $z_{tr}$ constraints. When $H_0$ is fixed, $z_{tr}$ is positively correlated with it, and the larger $H_0$ is, the larger the $z_{tr}$ is (Farooq & Ratra 2013; Farooq et al. 2017). Considering that the value of the nuisance parameter $H_0$ can affect the estimation of $z_{tr}$, we screened out $z_{tr}$ with $H_0$ as a free parameter from the total $z_{tr}$ set $(2004 - 2024)$, and then show it in Fig. 8. For convenience, we defined the $z_{tr}$ constraints selected by the free parameter $H_0$ as the screening condition as "screened $z_{tr}$ constraints". From Fig. 8, it can be found that the screened $z_{tr}$ constraints can be well described by a Gaussian function with the mean value 0.64 ($\bar{z}_{tr}$(free)) and the standard deviation 0.16 ($\sigma_{\bar{z}_{tr}}$(free)). Compared with the previous results ($\bar{z}_{tr}$(free) $= 0.65 \pm 0.16$), there is no significant change. All in all, the $z_{tr}$ constraints are closely related to many factors, such as data type, research method, redshift range and assumption. To clarify the details, more precisely measurements are needed for further research.

Recently, a possible correlation between the lens redshift and the inferred of $H_0(z)$ was found using time-delay cosmography of lensed quasars by the H0LiCOW collaboration (Wong et al. 2020). The statistical significance was approximately $1.9\sigma$. Subsequently, the addition of a new H0LiCOW lens (DES J0408-5354) by Millon et al. (2020) slightly weakened the trend to $1.7\sigma$. Inspired by this, Krishnan et al. (2020) obtained $H_0$ constraints for different redshift ranges ($z < 0.7$) by binning a joint dataset consisting of megamasers, CCs, SNe Ia and BAO according to redshift. They also found a similar $H_0$ descending trend with low significance in different cosmological models (Krishnan et al. 2020). To date, the same $H_0$ descending trend has been verified by multiple methods and datasets (Dainotti et al. 2021; Horstmann et al. 2022; Hu & Wang 2022a; Wu et al. 2022; Ó Colgáin et al. 2022; Jia et al. 2023, 2025; Montani et al. 2025a; Gao et al. 2025; Dilsiz et al. 2025). These researches hint that the Hubble constant $H_0$ might evolve with redshift. What caused the evolution is still unclear. There are many speculations about the possible reasons for the evolution of $H_0$, for instance the local void (Enqvist 2008; Garcia-Bellido & Haugbølle 2008; Keenan et al. 2013; Wang & Dai 2013; Mazurenko et al. 2025; Banik & Kalaitzidis 2025), cosmic anisotropy (Yadav 2023; Hu et al. 2024a; Yadav et al. 2024; Hu et al. 2024c), modified gravity (Capozziello et al. 2020a; Benetti et al. 2021; Escamilla et al. 2024), dynamic dark energy (Colgáin & Sheikh-Jabbari 2024; Giarè et al. 2024; Adame et al. 2025b; Montani et al. 2025a; Park & Ratra 2025), dark energy - dark matter interaction (Wang et al. 2016; Montani et al. 2025b) and so on. But there is no conclusion yet.

According to the research on $H_0$ redshift evolution, we know that starting from a certain moment in the late universe, the $H_0$ constraint began to deviate from the CMB result (Planck Collaboration et al. 2020a), gradually evolving into the current Hubble tension (Krishnan et al. 2020; Hu & Wang 2022a; Jia et al. 2023, 2025; Mazurenko et al. 2025). From the study of Krishnan et al. (2020), it can be found that the divergence of $H_0$ begins around redshift 0.50. Hu & Wang (2022a) reported a late-time transition of $H_0$; that is, $H_0$ changes from a low value to a high one from early to late cosmic time by combining the GP method and $H(z)$ measurements. The $H_0$ transition occurs around redshift 0.49, which is also where the divergence of $H_0$ begins. In addition, some studies have shown that the divergence of $H_0$ begins around 0.70 (Jia et al. 2023, 2025). Thus, these findings suggest that the Hubble tension might begin near the redshift interval of 0.49 to 0.70. Coincidentally, we find that the transition redshift ($\bar{z}_{tr}(\text{all}) = 0.65\pm$ 0.16 and $\bar{z}_{tr}(\text{free}) = 0.64\pm$ 0.16) obtained based on the statistical analysis from 2004 to 2024 are exactly within this range. Therefore, we suspect that Hubble tension might be related to this special period of cosmic evolution, when the Universe smoothly transitions from a decelerating expansion to an accelerating expansion. Previously, we have always believed that the Hubble tension was just a contradiction between the early-time and late-time universe. But the redshift evolution of the Hubble constant seems to tell us that the Hubble tension may also be a contradiction between different redshift intervals in the late-time universe. And combined with the history of cosmic evolution, we suspect that the Hubble tension might be closely related to this special period of cosmic evolution. Near the transition redshift $z_{tr}$, the proportion of dark energy increases slightly, causing the Hubble constant to evolve with redshift. There are many physical mechanisms that cause the increase in the dark energy percentage, such as dynamical dark energy (Colgáin & Sheikh-Jabbari 2024; Giarè et al. 2024; Adame et al. 2025b; Montani et al. 2025a; Park & Ratra 2025; Scherer et al. 2025) and dark energy - dark matter interaction (Wang et al. 2016; Montani et al. 2025b). From Planck + DR2 + DESY5 dataset, Scherer et al. (2025) found a transition from a phantom-like regime ($w <$ -1) at early times to a quintessence-like regime ($w >$ -1) today, driven by the negative values of the deviation parameter $\Delta$. The transition occurs at around redshift 0.50. Detailed information can be found in Figure 5 in literature (Scherer et al. 2025). In addition, an unknown physical mechanism might have occurred during the special period, exacerbating the accelerated expansion of the Universe and causing the current Hubble tension. The unknown mechanism might also be related to the special properties of dark matter and dark energy. Further research not only requires more precise observations to accurately constrain the transition redshift $z_{tr}$ and the redshift evolution behavior of Hubble constant, but also requires a deeper understanding of dark matter and dark energy. In summary, precise positioning of $z_{tr}$ might help to find the physical nature of the redshift evolution of the Hubble constant and the Hubble tension.

## 6 CONCLUSION

Transition redshift $z_{tr}$ is a special period in the history of cosmic evolution, when the Universe smoothly transitions from decelerating expansion to accelerating expansion. Determining the exact moment in which accelerated phase began is an interesting question. In the present paper, we constrain the transition redshift $z_{tr}$ utilizing the latest H(z) measurements (35 CCs, 20 BAOs and 5 DESI BAOs) and three kinds of methods ($\Lambda$CDM model, Cosmography, and GP method). By comparing the constraints given by different methods and datasets, we find that dataset and methodology can both affect the final constraints, with the latter having a stronger impact. Compared with the other two model-independent methods, the $\Lambda$CDM model prefers a larger $z_{tr}$ constraint. Different methods have different abilities to constrain the transition redshift $z_{tr}$. Through statistical analyses of the research results from 2004 to 2024, we find that all $z_{tr}$ constraints and the screened $z_{tr}$ constraints with free $H_0$ can be well described by Gaussian functions; that is $\bar{z}_{tr}(\text{all}) = 0.65 \pm 0.16$ and $\bar{z}_{tr}(\text{free}) = 0.64 \pm 0.16$. Coincidentally, these results overlap with the initial position of the redshift evolution of the Hubble constant. Therefore, we speculate that the origin of the Hubble tension might be associated with the special period. However, a reasonable physical mechanism to explain this coincidence and firmly link the two is lacking. In future research, we will pay more attention to studying the late-time evolution of the Universe, especially around redshift range (0.50, 0.70), to find a suitable physical explanation.

In summary, the determination of the transition redshift $z_{tr}$ is similar importance in modern cosmology as the Hubble constant $H_0$, deceleration parameter $q_0$, and cosmic constant $\Lambda$. Accurately constraining the redshift is crucial to understanding the evolutionary history of the late-time Universe and will provide new perspectives for exploring the redshift evolution of the Hubble constant and the physical nature of the Hubble tension.

## ACKNOWLEDGEMENTS

Anonymous reviewer provided many constructive comments, for which we are deeply grateful. This work was supported by the National Natural Science Foundation of China (grant No. 12273009, No. 12373026), Leading Innovation and Entrepreneurship Team of Zhejiang Province of China (grant No. 2023R01008), and Key R&D Program of Zhejiang, China (grant No. 2024SSYS0012).

## DATA AVAILABILITY

The data used in the paper are publicly available in Tables A1 and A2.

## REFERENCES

Abbott T. M. C., et al., 2019, Phys. Rev. Lett., 122, 171301
Abbott T. M. C., et al., 2024, ApJ, 973, L14
Abdalla E., et al., 2022, Journal of High Energy Astrophysics, 34, 49
Adame A. G., et al., 2025a, J. Cosmology Astropart. Phys., 2025, 124
Adame A. G., et al., 2025b, J. Cosmology Astropart. Phys., 2025, 021
Adame A. G., et al., 2025c, J. Cosmology Astropart. Phys., 2025, 012
Alam S., et al., 2017, MNRAS, 470, 2617
Anderson L., et al., 2014, MNRAS, 441, 24
Arjona R., Nesseris S., 2021, Phys. Rev. D, 103, 063537
Banik I., Kalaitzidis V., 2025, MNRAS, 540, 545
Bargiacchi G., Risaliti G., Benetti M., Capozziello S., Lusso E., Saccardi A., Signorini M., 2021, A&A, 649, A65
Benetti M., Capozziello S., Lambiase G., 2021, MNRAS, 500, 1795
Bengaly C. A. P., Alcaniz J. S., Pigozzo C., 2024, Phys. Rev. D, 109, 123533
Blake C., et al., 2012, MNRAS, 425, 405
Borghi N., Moresco M., Cimatti A., 2022, ApJ, 928, L4
Boubel P., Colless M., Said K., Staveley-Smith L., 2025, J. Cosmology Astropart. Phys., 2025, 066
Briffa R., Capozziello S., Said J. L., Mifsud J., Saridakis E. N., 2020, Classical and Quantum Gravity, 38, 055007
Brout D., et al., 2022, ApJ, 938, 110
Busca N. G., et al., 2013, A&A, 552, A96
Cai Y.-F., Capozziello S., De Laurentis M., Saridakis E. N., 2016, Reports on Progress in Physics, 79, 106901
Cao S., Khadka N., Ratra B., 2022a, MNRAS, 510, 2928
Cao S., Dainotti M., Ratra B., 2022b, MNRAS, 512, 439
Capozziello S., Ruchika Sen A. A., 2019, MNRAS, 484, 4484
Capozziello S., de Laurentis M., 2011, Phys. Rep., 509, 167
Capozziello S., Lazkoz R., Salzano V., 2011, Phys. Rev. D, 84, 124061
Capozziello S., Farooq O., Luongo O., Ratra B., 2014, Phys. Rev. D, 90, 044016
Capozziello S., Luongo O., Saridakis E. N., 2015, Phys. Rev. D, 91, 124037
Capozziello S., D'Agostino R., Luongo O., 2018, MNRAS, 476, 3924
Capozziello S., D'Agostino R., Luongo O., 2019, International Journal of Modern Physics D, 28, 1930016
Capozziello S., Benetti M., Spallicci A. D. A. M., 2020a, Foundations of Physics, 50, 893
Capozziello S., D'Agostino R., Luongo O., 2020b, MNRAS, 494, 2576
Capozziello S., Dunsby P. K. S., Luongo O., 2022, MNRAS, 509, 5399
Capozziello S., Sarracino G., De Somma G., 2024, Universe, 10, 140
Cattoën C., Visser M., 2007, Classical and Quantum Gravity, 24, 5985
Chen S. F., et al., 2024, MNRAS, 534, 544
Chuang C.-H., et al., 2013, MNRAS, 433, 3559
Cline J. M., Grojean C., Servant G., 1999, Phys. Rev. Lett., 83, 4245
Colgáin E. Ó., Sheikh-Jabbari M. M., 2024, arXiv e-prints, p. arXiv:2412.12905
Cunha J. V., Lima J. A. S., 2008, MNRAS, 390, 210
Dainotti M. G., De Simone B., Schiavone T., Montani G., Rinaldi E., Lambiase G., 2021, ApJ, 912, 150
Dainotti M. G., De Simone B. D., Schiavone T., Montani G., Rinaldi E., Lambiase G., Bogdan M., Ugale S., 2022, Galaxies, 10, 24
Dainotti M. G., Lenart A. Ł., Chraya A., Sarracino G., Nagataki S., Fraija N., Capozziello S., Bogdan M., 2023, MNRAS, 518, 2201
Dainotti M. G., et al., 2025, arXiv e-prints, p. arXiv:2501.11772
Damour T., Polyakov A. M., 1994, General Relativity and Gravitation, 26, 1171
Davis M., Efstathiou G., Frenk C. S., White S. D. M., 1985, ApJ, 292, 371
De Simone B., van Putten M. H. P. M., Dainotti M. G., Lambiase G., 2024, arXiv e-prints, p. arXiv:2411.05744
Delubac T., et al., 2015, A&A, 574, A59
Di Valentino E., et al., 2021, Classical and Quantum Gravity, 38, 153001
Dilsiz F. Ş., Deliduman C., Binici S. S., 2025, Physics of the Dark Universe, 48, 101943
Dunsby P. K. S., Luongo O., 2016, International Journal of Geometric Methods in Modern Physics, 13, 1630002
Eisenstein D. J., et al., 2005, ApJ, 633, 560
Eisenstein D. J., et al., 2011, AJ, 142, 72
Enqvist K., 2008, General Relativity and Gravitation, 40, 451
Escamilla L. A., Fiorucci D., Montani G., Di Valentino E., 2024, Physics of the Dark Universe, 46, 101652
Farooq O., Ratra B., 2013, ApJ, 766, L7
Farooq O., Crandall S., Ratra B., 2013a, Physics Letters B, 726, 72
Farooq O., Mania D., Ratra B., 2013b, ApJ, 764, 138
Farooq O., Ranjeet Madiyar F., Crandall S., Ratra B., 2017, ApJ, 835, 26
Favale A., Dainotti M. G., Gómez-Valent A., Migliaccio M., 2024, Journal of High Energy Astrophysics, 44, 323
Firmani C., Ghisellini G., Ghirlanda G., Avila-Reese V., 2005, MNRAS, 360, L1
Font-Ribera A., et al., 2014, J. Cosmology Astropart. Phys., 2014, 027
Foreman-Mackey D., Hogg D. W., Lang D., Goodman J., 2013, PASP, 125, 306
Gao J., Zhou Z., Du M., Zou R., Hu J., Xu L., 2024, MNRAS, 527, 7861

Gao D. H., Wu Q., Hu J. P., Yi S. X., Zhou X., Wang F. Y., Dai Z. G., 2025, A&A, 698, A215
Garcia-Bellido J., Haugbølle T., 2008, J. Cosmology Astropart. Phys., 2008, 003
Gaztañaga E., Cabré A., Hui L., 2009, MNRAS, 399, 1663
Giarè W., Najafi M., Pan S., Di Valentino E., Firouzjaee J. T., 2024, J. Cosmology Astropart. Phys., 2024, 035
Gómez-Valent A., Amendola L., 2018, J. Cosmology Astropart. Phys., 2018, 051
Gómez-Valent A., Favale A., Migliaccio M., Sen A. A., 2024, Phys. Rev. D, 109, 023525
Guimarães A. C. C., Cunha J. V., Lima J. A. S., 2009, J. Cosmology Astropart. Phys., 2009, 010
Guo J.-Q., Frolov A. V., 2013, Phys. Rev. D, 88, 124036
Haridasu B. S., Luković V. V., Moresco M., Vittorio N., 2018, J. Cosmology Astropart. Phys., 2018, 015
Horstmann N., Pietschke Y., Schwarz D. J., 2022, A&A, 668, A34
Hu J. P., Wang F. Y., 2022a, MNRAS, 517, 576
Hu J. P., Wang F. Y., 2022b, A&A, 661, A71
Hu J.-P., Wang F.-Y., 2023, Universe, 9, 94
Hu J. P., Wang F. Y., Dai Z. G., 2021, MNRAS, 507, 730
Hu J. P., Wang Y. Y., Hu J., Wang F. Y., 2024a, A&A, 681, A88
Hu J. P., Hu J., Jia X. D., Gao B. Q., Wang F. Y., 2024b, A&A, 689, A215
Hu J. P., Jia X. D., Hu J., Wang F. Y., 2024c, ApJ, 975, L36
Jesus J. F., Holanda R. F. L., Pereira S. H., 2018, J. Cosmology Astropart. Phys., 2018, 073
Jesus J. F., Valentim R., Escobal A. A., Pereira S. H., 2020, J. Cosmology Astropart. Phys., 2020, 053
Jia X. D., Hu J. P., Yang J., Zhang B. B., Wang F. Y., 2022, MNRAS, 516, 2575
Jia X. D., Hu J. P., Wang F. Y., 2023, A&A, 674, A45
Jia X. D., Hu J. P., Yi S. X., Wang F. Y., 2025, ApJ, 979, L34
Jiao K., Borghi N., Moresco M., Zhang T.-J., 2023, ApJS, 265, 48
Jimenez R., Loeb A., 2002, ApJ, 573, 37
Jimenez R., Moresco M., Verde L., Wandelt B. D., 2023, J. Cosmology Astropart. Phys., 2023, 047
Kalbouneh B., Marinoni C., Maartens R., 2024, J. Cosmology Astropart. Phys., 2024, 069
Kalbouneh B., Santiago J., Marinoni C., Maartens R., Clarkson C., Sarma M., 2025, J. Cosmology Astropart. Phys., 2025, 076
Keenan R. C., Barger A. J., Cowie L. L., 2013, ApJ, 775, 62
Komatsu E., et al., 2011, ApJS, 192, 18
Koussour M., Myrzakulov N., Ali M. K. M., 2024, Journal of High Energy Astrophysics, 42, 96
Krishnan C., Colgáin E. Ó., Ruchika A. A. S., Sheikh-Jabbari M. M., Yang T., 2020, Phys. Rev. D, 102, 103525
Krishnan C., Mohayaee R., Colgáin E. Ó., Sheikh-Jabbari M. M., Yin L., 2021, Classical and Quantum Gravity, 38, 184001
Kroupa P., et al., 2023, in School and Workshops on Elementary Particle Physics and Gravity. p. 231 (arXiv:2309.11552), doi:10.48550/arXiv.2309.11552
Kumar D., Jain D., Mahajan S., Mukherjee A., Rana A., 2023, International Journal of Modern Physics D, 32, 2350039
Li E.-K., Du M., Xu L., 2020, MNRAS, 491, 4960
Li Z., Zhang B., Liang N., 2023, MNRAS, 521, 4406
Liang E., Zhang B., 2005, ApJ, 633, 611
Liang N., Li Z., Xie X., Wu P., 2022, ApJ, 941, 84
Liao K., Shafieloo A., Keeley R. E., Linder E. V., 2019, ApJ, 886, L23
Liu Y., Liang N., Xie X., Yuan Z., Yu H., Wu P., 2022, ApJ, 935, 7
Liu Y., Yu H., Wu P., 2024a, Phys. Rev. D, 110, L021304
Liu Y., Wang B., Yu H., Wu P., 2024b, MNRAS, 533, 244
Lopez-Hernandez M., De-Santiago J., 2025, J. Cosmology Astropart. Phys., 2025, 026
Luongo O., Muccino M., 2024, arXiv e-prints, p. arXiv:2412.18493
Lusso E., Piedipalumbo E., Risaliti G., Paolillo M., Bisogni S., Nardini E., Amati L., 2019, A&A, 628, L4
Malekjani M., Mc Conville R., Ó Colgáin E., Pourojaghi S., Sheikh-Jabbari M. M., 2024, European Physical Journal C, 84, 317
Mazurenko S., Banik I., Kroupa P., 2025, MNRAS, 536, 3232
Melia F., Yennapureddy M. K., 2018, J. Cosmology Astropart. Phys., 2018, 034
Milgrom M., 1983, ApJ, 270, 365
Millon M., et al., 2020, A&A, 639, A101
Mishra S. S., Kavya N. S., Sahoo P. K., Venkatesha V., 2025, Physics of the Dark Universe, 47, 101759
Montani G., Carlevaro N., Dainotti M. G., 2025a, Physics of the Dark Universe, 48, 101847
Montani G., Carlevaro N., Escamilla L. A., Di Valentino E., 2025b, Physics of the Dark Universe, 48, 101848
Moresco M., 2015, MNRAS, 450, L16
Moresco M., et al., 2012, J. Cosmology Astropart. Phys., 2012, 006
Moresco M., et al., 2016, J. Cosmology Astropart. Phys., 2016, 014
Moresco M., Jimenez R., Verde L., Cimatti A., Pozzetti L., 2020, ApJ, 898, 82
Moresco M., et al., 2022, Living Reviews in Relativity, 25, 6
Muccino M., Luongo O., Jain D., 2023, MNRAS, 523, 4938
Myrzakulov R., 2011, European Physical Journal C, 71, 1752
Myrzakulov Y., Donmez O., Koussour M., Alizhanov D., Bekchanov S., Rayimbaev J., 2024, Physics of the Dark Universe, 46, 101614
Nakamura T., Chiba T., 1999, MNRAS, 306, 696
Neveux R., et al., 2020, MNRAS, 499, 210
Ó Colgáin E., Sheikh-Jabbari M. M., Solomon R., Bargiacchi G., Capozziello S., Dainotti M. G., Stojkovic D., 2022, Phys. Rev. D, 106, L041301
Ó Colgáin E., Sheikh-Jabbari M. M., Solomon R., Dainotti M. G., Stojkovic D., 2024, Physics of the Dark Universe, 44, 101464
Ó. Colgáin E., Pourojaghi S., Sheikh-Jabbari M. M., Sherwin D., 2025, European Physical Journal C, 85, 124
Overduin J. M., Wesson P. S., 1997, Phys. Rep., 283, 303
Padmanabhan T., 2003, Phys. Rep., 380, 235
Park C.-G., Ratra B., 2025, arXiv e-prints, p. arXiv:2501.03480
Pedregosa F., et al., 2011, Journal of Machine Learning Research, 12, 2825
Peebles P. J., Ratra B., 2003, Reviews of Modern Physics, 75, 559
Perivolaropoulos L., Skara F., 2022, New Astron. Rev., 95, 101659
Planck Collaboration et al., 2014, A&A, 571, A16
Planck Collaboration et al., 2020a, A&A, 641, A6
Planck Collaboration et al., 2020b, A&A, 641, A6
Pourojaghi S., Malekjani M., Davari Z., 2025, MNRAS, 537, 436
Rahman S. F. u., 2023, Gravitation and Cosmology, 29, 177
Randall L., Sundrum R., 1999, Phys. Rev. Lett., 83, 4690
Rani N., Jain D., Mahajan S., Mukherjee A., Pires N., 2015, J. Cosmology Astropart. Phys., 2015, 045
Rasmussen C. E., Williams C. K. I., 2006, Gaussian Processes for Machine Learning
Ratsimbazafy A. L., Loubser S. I., Crawford S. M., Cress C. M., Bassett B. A., Nichol R. C., Väisänen P., 2017, MNRAS, 467, 3239
Riess A. G., Breuval L., 2024, in de Grijs R., Whitelock P. A., Catelan M., eds, IAU Symposium Vol. 376, IAU Symposium. pp 15–29 (arXiv:2308.10954), doi:10.1017/S1743921323003034
Riess A. G., et al., 1998, AJ, 116, 1009
Riess A. G., et al., 2004, ApJ, 607, 665
Riess A. G., et al., 2007, ApJ, 659, 98
Riess A. G., et al., 2011, ApJ, 730, 119
Riess A. G., et al., 2022, ApJ, 934, L7
Roos M., 2012, Journal of Modern Physics, 3, 1152

Rubin D., et al., 2023, arXiv e-prints, p. arXiv:2311.12098
Sah A., Rameez M., Sarkar S., Tsagas C., 2024, arXiv e-prints, p. arXiv:2411.10838
Salehi A., Hatami H., 2022, European Physical Journal C, 82, 1165
Scherer M., Sabogal M. A., Nunes R. C., De Felice A., 2025, arXiv e-prints, p. arXiv:2504.20664
Schulz E., Speekenbrink M., Krause A., 2018, Journal of Mathematical Psychology, 85, 1
Scolnic D. M., et al., 2018, ApJ, 859, 101
Seikel M., Clarkson C., Smith M., 2012, J. Cosmology Astropart. Phys., 2012, 036
Silk J., et al., 2010, Particle Dark Matter: Observations, Models and Searches. Cambridge Univ. Press, Cambridge, doi:10.1017/CBO9780511770739
Simon J., Verde L., Jimenez R., 2005, Phys. Rev. D, 71, 123001
Smee S. A., et al., 2013, AJ, 146, 32
Sudharani L., Bamba K., Kavya N. S., Venkatesha V., 2024, Physics of the Dark Universe, 45, 101522
Tomasetti E., et al., 2023a, A&A, 679, A96
Tomasetti E., et al., 2023b, A&A, 679, A96
Vagnozzi S., 2023, Universe, 9, 393
Velasquez-Toribio A. M., Fabris J. C., 2022, Brazilian Journal of Physics, 52, 115
Velasquez-Toribio A. M., Magnago A. d. R., 2020, European Physical Journal C, 80, 562
Visser M., 2004, Classical and Quantum Gravity, 21, 2603
Visser M., 2015, Classical and Quantum Gravity, 32, 135007
Volkov M. S., 2012, Phys. Rev. D, 86, 061502
Wang F. Y., Dai Z. G., 2006, MNRAS, 368, 371
Wang F. Y., Dai Z. G., 2013, Nature Physics, 9, 465
Wang F. Y., Dai Z. G., Liang E. W., 2015, New Astron. Rev., 67, 1
Wang B., Abdalla E., Atrio-Barandela F., Pavón D., 2016, Reports on Progress in Physics, 79, 096901
Wang Y., et al., 2017, MNRAS, 469, 3762
Wang F. Y., Hu J. P., Zhang G. Q., Dai Z. G., 2022, ApJ, 924, 97
Wang B., López-Corredoira M., Wei J.-J., 2024, MNRAS, 527, 7692
Weinberg S., 1972, Gravitation and Cosmology: Principles and Applications of the General Theory of Relativity, by Steven Weinberg, pp. 688. ISBN 0-471-92567-5. Wiley-VCH , July 1972.
Weinberg S., 1989, Reviews of Modern Physics, 61, 1
Wong K. C., et al., 2020, MNRAS, 498, 1420
Wu Q., Zhang G.-Q., Wang F.-Y., 2022, MNRAS, 515, L1
Xu L., Li W., Lu J., 2009, J. Cosmology Astropart. Phys., 2009, 031
Xu B., Xu J., Zhang K., Fu X., Huang Q., 2024, MNRAS, 530, 5091
Yadav V., 2023, Physics of the Dark Universe, 42, 101365
Yadav V., Yadav S. K., Rajpal 2024, Physics of the Dark Universe, 46, 101626
Yang Y., Ren X., Wang Q., Lu Z., Zhang D., Cai Y.-F., Saridakis E. N., 2024, Science Bulletin, 69, 2698
Yu H., Ratra B., Wang F.-Y., 2018, ApJ, 856, 3
Zhang C., Zhang H., Yuan S., Liu S., Zhang T.-J., Sun Y.-C., 2014, Research in Astronomy and Astrophysics, 14, 1221
du Mas des Bourboux H., et al., 2017, A&A, 608, A130

This paper has been typeset from a TEX/LATEX file prepared by the author.

**Table A1.** $H(z)$ measurements from Cosmic Chronometer (in units of km $s^{-1}Mpc^{-1}$).

| No. | $z$ | $H(z)$ | Ref. | No. | $z$ | $H(z)$ | Ref. |
|---|---|---|---|---|---|---|---|
| (1) | 0.07 | $69.0 \pm 19.6$ | Zhang et al. (2014) | (2) | 0.09 | $69.0 \pm 12.0$ | Simon et al. (2005) |
| (3) | 0.12 | $68.6 \pm 26.2$ | Zhang et al. (2014) | (4) | 0.17 | $83.0 \pm 8.0$ | Simon et al. (2005) |
| (5) | 0.179 | $75.0 \pm 4.0$ | Moresco et al. (2012) | (6) | 0.199 | $75.0 \pm 5.0$ | Moresco et al. (2012) |
| (7) | 0.2 | $72.9 \pm 29.6$ | Zhang et al. (2014) | (8) | 0.27 | $77.0 \pm 14.0$ | Simon et al. (2005) |
| (9) | 0.28 | $88.8 \pm 36.6$ | Zhang et al. (2014) | (10) | 0.352 | $83.0 \pm 14.0$ | Moresco et al. (2012) |
| (11) | 0.3802 | $83.0 \pm 13.5$ | Moresco et al. (2016) | (12) | 0.4 | $95.0 \pm 17.0$ | Simon et al. (2005) |
| (13) | 0.4004 | $77.0 \pm 10.2$ | Moresco et al. (2016) | (14) | 0.4247 | $87.1 \pm 11.2$ | Moresco et al. (2016) |
| (15) | 0.4497 | $92.8 \pm 12.9$ | Moresco et al. (2016) | (16) | 0.47 | $89.0 \pm 50$ | Ratsimbazafy et al. (2017) |
| (17) | 0.4783 | $80.9 \pm 9.0$ | Moresco et al. (2016) | (18) | 0.48 | $97.0 \pm 62.0$ | Ratsimbazafy et al. (2017) |
| (19) | 0.593 | $104.0 \pm 13.0$ | Moresco et al. (2012) | (20) | 0.68 | $92.0 \pm 8.0$ | Moresco et al. (2012) |
| (21) | 0.75 | $98.8 \pm 33.6$ | Borghi et al. (2022) | (22) | 0.75 | $105.0 \pm 7.9$ | Jimenez et al. (2023) |
| (23) | 0.781 | $105.0 \pm 12.0$ | Moresco et al. (2012) | (24) | 0.80 | $113.1 \pm 15.1$ | Jiao et al. (2023) |
| (25) | 0.875 | $125.0 \pm 17.0$ | Moresco et al. (2012) | (26) | 0.88 | $90.0 \pm 40.0$ | Ratsimbazafy et al. (2017) |
| (27) | 0.9 | $117.0 \pm 23.0$ | Simon et al. (2005) | (28) | 1.037 | $154.0 \pm 20.0$ | Moresco et al. (2012) |
| (29) | 1.26 | $135.0 \pm 65$ | Tomasetti et al. (2023b) | (30) | 1.3 | $168.0 \pm 17.0$ | Simon et al. (2005) |
| (31) | 1.363 | $160.0 \pm 33.6$ | Moresco (2015) | (32) | 1.43 | $177.0 \pm 18.0$ | Simon et al. (2005) |
| (33) | 1.53 | $140.0 \pm 14.0$ | Simon et al. (2005) | (34) | 1.75 | $202.0 \pm 40.0$ | Simon et al. (2005) |
| (35) | 1.965 | $186.5 \pm 50.4$ | Moresco (2015) | | | | |

**Table A2.** $H(z)$ measurements from the BAO measurements including 5 DESI BAOs (in units of km $s^{-1}Mpc^{-1}$).

| No. | $z$ | $H(z)$ | Ref. | No. | $z$ | $H(z)$ | Ref. |
|---|---|---|---|---|---|---|---|
| **DESI:** | | | | | | | |
| (1) | 0.51 | $97.21 \pm 2.83$ | Adame et al. (2025c) | (2) | 0.71 | $101.57 \pm 3.04$ | Adame et al. (2025c) |
| (3) | 0.93 | $114.07 \pm 2.24$ | Adame et al. (2025c) | (4) | 1.32 | $147.58 \pm 4.49$ | Adame et al. (2025c) |
| (5) | 2.33 | $239.38 \pm 4.80$ | Adame et al. (2025a) | | | | |
| **Other:** | | | | | | | |
| (1) | 0.24 | $79.69 \pm 2.99$ | Gaztañaga et al. (2009) | (2) | 0.36 | $79.93 \pm 3.39$ | Wang et al. (2017) |
| (3) | 0.38 | $81.50 \pm 1.90$ | Alam et al. (2017) | (4) | 0.40 | $82.04 \pm 2.03$ | Wang et al. (2017) |
| (5) | 0.43 | $86.45 \pm 3.68$ | Gaztañaga et al. (2009) | (6) | 0.44 | $84.81 \pm 1.83$ | Wang et al. (2017) |
| (7) | 0.48 | $87.79 \pm 2.03$ | Wang et al. (2017) | (8) | 0.51 | $90.40 \pm 1.90$ | Alam et al. (2017) |
| (9) | 0.56 | $93.33 \pm 2.32$ | Wang et al. (2017) | (10) | 0.57 | $87.60 \pm 7.80$ | Chuang et al. (2013) |
| (11) | 0.57 | $96.80 \pm 3.40$ | Anderson et al. (2014) | (12) | 0.59 | $98.48 \pm 3.19$ | Wang et al. (2017) |
| (13) | 0.60 | $87.90 \pm 6.10$ | Blake et al. (2012) | (14) | 0.61 | $97.30 \pm 2.10$ | Alam et al. (2017) |
| (15) | 0.64 | $98.82 \pm 2.99$ | Wang et al. (2017) | (16) | 1.48 | $153.81 \pm 6.39$ | Neveux et al. (2020) |
| (17) | 2.30 | $224.0 \pm 8.0$ | Busca et al. (2013) | (18) | 2.34 | $223.0 \pm 7.0$ | Delubac et al. (2015) |
| (19) | 2.36 | $226.0 \pm 8.0$ | Font-Ribera et al. (2014) | (20) | 2.40 | $227.8 \pm 5.61$ | du Mas des Bourboux et al. (2017) |

## APPENDIX A: ADDITIONAL MATERIALS

Tables A1 and A2 show the H(z) measurements used in this paper. Table A3 shows the $z_{tr}$ constraints collected from 2004 to 2024.

**Table A3.** Constraints of the transition redshift $z_{tr}$ obtained by different methods and different datasets.

| Year | $z_{tr}$ | method | Ref. | Year | $z_{tr}$ | method | Ref. |
|---|---|---|---|---|---|---|---|
| 2004 | $0.46^{+0.13}_{-0.13}$ | SNe Ia (a) | Riess et al. (2004) | 2018 | $0.81^{+0.09}_{-0.09}$ | H(z) + SNe Ia (e) | Jesus et al. (2018) |
| 2005 | $0.73^{+0.09}_{-0.09}$ | GRBs + SNe Ia (b) | Firmani et al. (2005) | 2018 | $0.87^{+0.06}_{-0.06}$ | H(z) + SNe Ia (e) | Jesus et al. (2018) |
| 2005 | 0.40 | GRBs + SNe Ia (c) | Firmani et al. (2005) | 2018 | $0.97^{+0.06}_{-0.06}$ | H(z) + SNe Ia (e) | Jesus et al. (2018) |
| 2005 | 0.55 | GRBs + SNe Ia (d) | Firmani et al. (2005) | 2018 | $0.57^{+0.27}_{-0.23}$ | CCs + two ly$\alpha$ (j) | Yu et al. (2018) |
| 2005 | $0.78^{+0.32}_{-0.23}$ | GRBs (b) | Liang & Zhang (2005) | 2018 | $0.46^{+0.32}_{-0.12}$ | H(z) (j) | Yu et al. (2018) |
| 2006 | $0.69^{+0.11}_{-0.12}$ | GRBs (b) | Wang & Dai (2006) | 2018 | $0.55^{+0.23}_{-0.20}$ | CCs (j) | Yu et al. (2018) |
| 2006 | $0.61^{+0.05}_{-0.06}$ | GRBs + SNe Ia (b) | Wang & Dai (2006) | 2018 | $0.44^{+0.56}_{-0.11}$ | H(z) (j) | Yu et al. (2018) |
| 2007 | $0.43^{+0.07}_{-0.07}$ | SNe Ia (a) | Riess et al. (2007) | 2018 | $0.64^{+0.12}_{-0.09}$ | H(z) + SNe Ia (j) | Haridasu et al. (2018) |
| 2008 | $0.61^{+3.68}_{-0.21}$ | SN LS (e) | Cunha & Lima (2008) | 2020 | $0.59^{+0.12}_{-0.11}$ | H(z) (j) | Jesus et al. (2020) |
| 2008 | $0.43^{+0.09}_{-0.05}$ | SNe Ia (e) | Cunha & Lima (2008) | 2020 | $0.68^{+0.11}_{-0.08}$ | SNe Ia (j) | Jesus et al. (2020) |
| 2008 | $0.60^{+0.28}_{-0.09}$ | SNe Ia (e) | Cunha & Lima (2008) | 2020 | $0.63^{+0.02}_{-0.02}$ | Planck (b) | Planck Collaboration et al. (2020a) |
| 2009 | $0.71^{+0.08}_{-0.08}$ | SNe Ia (b) | Guimarães et al. (2009) | 2020 | $0.70^{+0.30}_{-0.30}$ | H(z) + SNe Ia (b) | Velasquez-Toribio & Magnago (2020) |
| 2009 | $0.49^{+0.27}_{-0.09}$ | SNe Ia (a) | Guimarães et al. (2009) | 2021 | $0.65^{+0.03}_{-0.16}$ | H(z) + BAOs + SNe Ia (e) | Capozziello et al. (2022) |
| 2009 | $0.46^{+0.40}_{-0.28}$ | SNe Ia (a) | Guimarães et al. (2009) | 2021 | $0.57^{+0.37}_{-0.12}$ | H(z) (e) | Capozziello et al. (2022) |
| 2009 | $0.48^{+0.36}_{-0.11}$ | SNe Ia (a) | Guimarães et al. (2009) | 2021 | $1.02^{+0.01}_{-0.17}$ | H(z) + BAOs + SNe Ia (e) | Capozziello et al. (2022) |
| 2009 | $0.52^{+0.21}_{-0.08}$ | SNe Ia (a) | Guimarães et al. (2009) | 2021 | $0.60^{+0.12}_{-0.26}$ | H(z) (e) | Capozziello et al. (2022) |
| 2009 | $0.61^{+0.11}_{-0.07}$ | H(z) + BAOs + SNe Ia (a) | Xu et al. (2009) | 2022 | $0.43^{+0.04}_{-0.04}$ | H(z) + BAOs + SNe Ia (k) | Salehi & Hatami (2022) |
| 2009 | $0.59^{+0.09}_{-0.06}$ | H(z) + BAOs + SNe Ia (a) | Xu et al. (2009) | 2023 | $0.59^{+0.33}_{-0.33}$ | H(z) (l) | Kumar et al. (2023) |
| 2009 | $0.95^{+0.11}_{-0.08}$ | H(z) + BAOs + SNe Ia (a) | Xu et al. (2009) | 2023 | $0.62^{+0.58}_{-0.76}$ | H(z) (m) | Kumar et al. (2023) |
| 2013 | $0.82^{+0.08}_{-0.08}$ | BAOs (b) | Busca et al. (2013) | 2023 | $0.85^{+0.12}_{-0.12}$ | SNe Ia (l) | Kumar et al. (2023) |
| 2013 | $0.74^{+0.05}_{-0.05}$ | H(z) (*) | Farooq & Ratra (2013) | 2023 | $0.72^{+0.05}_{-0.05}$ | CCs + SNe Ia + ISW (b) | Rahman (2023) |
| 2013 | $0.74^{+0.04}_{-0.04}$ | H(z) (*) | Farooq et al. (2013a) | 2023 | $0.62^{+0.08}_{-0.13}$ | H(z) (n) | Muccino et al. (2023) |
| 2014 | $0.77^{+0.18}_{-0.18}$ | H(z) + SNe Ia (f) | Capozziello et al. (2014) | 2023 | $0.70^{+0.09}_{-0.04}$ | H(z) (e) | Muccino et al. (2023) |
| 2015 | $0.64^{+0.03}_{-0.03}$ | SNe Ia (g) | Capozziello et al. (2015) | 2023 | $0.81^{+0.08}_{-0.05}$ | H(z) (e) | Muccino et al. (2023) |
| 2015 | $0.25^{+0.35}_{-0.27}$ | SNe Ia (g) | Capozziello et al. (2015) | 2023 | $0.70^{+0.08}_{-0.06}$ | GRBs (e) | Muccino et al. (2023) |
| 2015 | 0.98 | AG + SL + SNe Ia (e) | Rani et al. (2015) | 2023 | $0.71^{+0.07}_{-0.07}$ | GRBs (e) | Muccino et al. (2023) |
| 2015 | 0.96 | AG + SL + SNe Ia (e) | Rani et al. (2015) | 2024 | 0.60 | H(z) + BAOs + SNe Ia (o) | Myrzakulov et al. (2024) |
| 2015 | 0.60 | AG + SL + SNe Ia (e) | Rani et al. (2015) | 2024 | 0.78 | H(z) + BAOs + SNe Ia (o) | Myrzakulov et al. (2024) |
| 2016 | $0.64^{+0.11}_{-0.06}$ | H(z) (h) | Moresco et al. (2016) | 2024 | 0.66 | H(z) + BAOs + SNe Ia (o) | Myrzakulov et al. (2024) |
| 2016 | $0.40^{+0.10}_{-0.10}$ | H(z) (i) | Moresco et al. (2016) | - | - | - | - |
| 2017 | $0.72^{+0.05}_{-0.05}$ | H(z) (*) | Farooq et al. (2017) | - | - | - | - |
| 2017 | $0.84^{+0.03}_{-0.03}$ | H(z) (*) | Farooq et al. (2017) | - | - | - | - |
| 2017 | $0.72^{+0.09}_{-0.09}$ | H(z) (b) | Farooq et al. (2017) | - | - | - | - |
| 2017 | $0.83^{+0.06}_{-0.06}$ | H(z) (b) | Farooq et al. (2017) | - | - | - | - |

Note: (a) Cosmography; (b) ΛCDM; (c) $w_0$CDM; (d) $w_z$CDM; (e) Linear parametrization; (f) f(R) gravity; (g) f(T) gravity; (h) oΛCDM; (i) Piecewise linear fit; (j) Gaussian Process; (k) Chameleon model; (l) Phase space portrait; (m) Cosmic triangle; (n) Bezier curve; (o) f(Q + $L_m$) gravity; (*) Statistical results.

Abb.: SN LS: Superluminous supernova; AG: Age of galaxies; SL: Strong lensing; ISW: Integrated Sachs-Wolfe effect.